Spatial resolution optimization of a cooling-down thermal imaging method to reveal hidden academic frescoes

Tanguy Davin, Bruno Serio, Géraldine Guida, Vincent Pina

Spatial resolution optimization of a cooling-down thermal imaging method to reveal hidden academic frescoes

Tanguy Davin, Bruno Serio, Géraldine Guida, Vincent Pina
Laboratoire Energétique Mécanique Electromagnétisme (LEME), EA 4416, Université Paris Ouest Nanterre La Défense, 50 rue de Sèvres, 92410 Ville d'Avray, France
tdavin@u-paris10.fr (corresponding author), bserio@u-paris10.fr, gguida@u-paris10.fr, vpina@u-paris10.fr

ABSTRACT

A safe cooling-down infrared thermography technique was considered to reveal paintings covered by a limewash layer for cultural heritage investigations. The transient infrared image sequence permits to reconstitute the subsurface pattern by processing the thermal contrast. Given the interest in detection methods, we propose a theoretical optimization study of the spatial resolution of the method. This analysis, achieved with thermal simulations, is based on both the thermal sensibility and a specific formal spatial resolution criterion. Considering a bar pattern painting covered by a 0.5 mm thick limewash, we have shown a thermal sensibility up to 1.5 K. This value is about 75 times bigger than the thermal noise threshold of the used camera. The proposed spatial resolution criterion allows to establish optimal temporal settings giving the sharpest thermal contrast image. An academic hidden painting sample was especially made to validate this theoretical approach. Results show the suitability of the method to perfectly reveal hidden patterns and confirm the spatial resolution estimations predicted using the proposed theoretical model. Simulated and experimental thermal contrast profiles are in good agreement.

Key-words: Infrared imaging; Cooling-down thermography; Thermal contrast optimization; Painting thermo-physical properties; Cultural heritage diagnostics; Defect analyses

1. INTRODUCTION

The study of frescoes is a key interest for the understanding of our history and the purpose of arts. There are arguments for the existence of numerous extensive hidden areas below the surface of the walls such as churches or old buildings of historical and architectural place. Indeed, numerous frescoes or paintings have been covered by an opacifiant layer for historical reasons such as political or religious events. These kinds of layer are generally made of lime or plaster diluted in water.

Optical techniques are powerful and versatile tools for the diagnosis of works of art. Numerous studies have considered techniques for restoration issues, once the paintings are discovered. For this purpose, some authors have focused on the pigments identification using various spectral methods [1][2][3]. Others studies have considered the material structure inspection of the paintings highlighting defects[4][5][6][7], earlier paintings restorations, underdrawings or *pentimenti* [8][9], and even controversial signatures[10]. Actually, there are numerous methods applicable for the detection of the presence of a work of art such as frescoes or mosaics.

The physical principles of methods for detecting objects buried in a wall made of lime or plaster depend of the used radiation. For instance, THz reflectometry can reveal wall structural discontinuities for the analysis of depths of interest (up to a few millimeters) [11][12]. Some particular materials such as graphite, metallic or dielectric patterns covered by a layer of pigments or plaster have been revealed using THz reflectometry and presented in reference [2]. Paintings hidden under a gesso layer was also recovered with the same method [13]. The use of terahertz radiations seems promising and is being developed in the last two decades but the pixels inspection number is still limited (object scanned point by point) so the acquisition requires a scanner and might be long. Furthermore, the THz sources needed to illuminate the scene are cumbersome, dear and limited in power. Therefore, the overall cost of this technology is still high.

Infrared methods are usually used in non-destructive testing of materials for inspecting or identifying defects using an either passive or active approach [14][15]. Passive thermal imaging methods are based on the fact that the features of interest are at a higher or lower temperature than the background. They have been used for a long time to analyze paintings in order to find sketches or previous drawings since they are easily implemented and totally safe [16]. However, investigating on plaster-like walls is more delicate by using passive infrared thermography since in steady state, the thermal gradient at the surface of the studied object is low. A paint layer covered by a layer made of plaster or lime for instance might be hard to be detected using a passive method.

Active infrared thermal imaging methods are also often used to inspect materials as a non-destructive approach[17]. Most of these methods are applied to reveal defects inside material structures[18][19][20]. The classical active thermography method used to probe this kind of layers consists in exciting the surface using high power photographic flashes or halogen lamps for heating. The thermal excitation is either a pulse/step (depending on its duration) or a periodic heating. The response of the thermally excited surface is recorded using a thermographic camera. For a heat pulse/step, the temperature rise or decay or both are then analyzed while for a periodic source, the amplitude and phase of the surface temperature are demodulated using a specific algorithm (lock-in or pulsed phase thermography).

In this paper a cooling-down infrared imaging method is carried out for the detection of a painting and its contour. Only a few similar studies were conducted, to discover plastered mosaics [21][22]. In particular, some tesserae pieces covered by a 1 mm lime mortar layer were discovered, using a pulse thermography method improved by processing image algorithm[21]. The detection for consequently thicker covering layers (up to 3.5 cm) was also demonstrated[22]. The coupling of measurements with an inverse method also permitted to identify some features as mosaic thickness, location or thermal properties. The covering layer considered for the present study, about 0.5 mm thick, is relatively thin compared to those hiding mosaics, but our goal is to reveal the hidden pattern. Also, the painting layer is highly thinner than the mosaics pieces.

The proposed experimental method is based on the processing of an infrared frame sequence acquired using a high sensitive pre-triggered MWIR FPA camera at high speed rate during the cooling-down occurring after application of a heat flux stimulation. The thermal diffusion inside the plastered fresco was computed after an analysis of the thermo-physical properties.

The thermal surface contrast, referenced to the end of the thermal stimulation, is defined to highlight the subsurface objects. The thermal contrast difference is defined as the criterion representing the thermal sensibility of the method. It is compared to the camera NETD to check the possibility of detection. As expressed in reference[23], the aptitude to reveal subsurface defects by pulsed thermography must be optimized by considering the time

dependence of the thermal system response. In this study, we have investigated the evolution of the thermal contrast for the proposed cooling-down method. This analysis, showing the thermal sensibility of the method, is important but results have revealed that the thermal diffusion that deteriorates the spatial resolution has to be considered as well. Therefore, a second criterion has been proposed to assess the influence of the processing time on the quality of the painting revelation by the thermal contrast function. This second criterion is defined by computing the surface temperature gradient relative to the maximum value. The combination of these two criteria highlights the choice of an optimum time value to process the infrared sequence giving the best thermal contrast image. This theoretical approach could be used to characterize the spatial resolution of all active thermography methods for defects detection. A bar pattern painting sample covered by limewash was realized to experimentally validate the method capabilities, in terms of presence detection and spatial resolution.

2. METHOD PRINCIPLE AND THERMO-PHYSICAL CHARACTERIZATION

2.1 Method principle

When the surface of the region of interest is heated using an external heat source, thermal waves flow inside the sample by thermal diffusion. Since the diffusion rate is affected by the existence of non-uniform thermal properties, the surface temperature over embedded paint layers will differ from the reference surrounding area.

However, the spectral nature of the source should be taken into account to understand the thermal excitation process in some cases. Indeed, the surface radiations are reflected, absorbed and possibly transmitted to deeper layers. Reflected radiations are added to the surface thermal emission and acts as a constant background that reduces the dynamic of the thermal imager. In this case, the absorbed part represents the required thermal surface excitation. The resulting heat flux propagated by thermal diffusion inside a wall depends on the absorption coefficient value of the limewash/plaster which is about 0.9 in the infrared band of a blackbody source at 500 °C for which the wavelength of maximum emission is 3.75 µm [12][24].

The transmitted radiations part could be used to generate a direct interface excitation as it was described in a previous work[25]. The spectral transmission of limewash and various pigments layers were previously measured. Since those materials are semi-transparent in far-infrared, their specific spectral signatures could be used to distinguish them from each other[26]. Considering spectroscopy measurements published in the previous reference, we estimate that only 0.01% of the total flux emitted by the used blackbody will be transmitted through the limewash layer. Consequently, the internal bulk absorption through the limewash was neglected in the current study and only an absorbed surface heat flux was taken into account for simulations presented in section 3. Figure 1 shows the principle of the radiative-conductive flux conversion used to thermally stimulate the buried painting layers.

We have chosen a black body source at 500 °C to excite the surface of the academic sample under test. In this configuration, the corresponding thermal flux absorbed at the sample surface is reasonably low, about 650 W/m². This mid-infrared thermal emission should not affect the integrity of the valuable sample and the source does not generate intense visible light such as halogen lamp sources commonly forbidden in historical places. Furthermore, in order to accurately detect the surface temperature singularities, we have used a high

resolution and high-speed infrared camera combined with a specific image processing to improve the signal-to-noise ratio, in particular by averaging images as a boxcar filter.

The used mid-IR camera detects the radiosity of the limewash surface. This flux is composed of the surface emission (represented in thick green in Figure 1) and the environment radiations reflection, mostly emitted from the black body during excitation. The component of the reflection on the sample surface overrides the small surface emission radiation. This is inconvenient for our application as the surface effects are not of interest. A large aperture mechanical shutter was used to stop the heating excitation. The camera was pre-triggered to record the sequence starting before the shutter was closed. The signal processing was done from the recorded sequence of infrared images selecting the transient cooling-down.

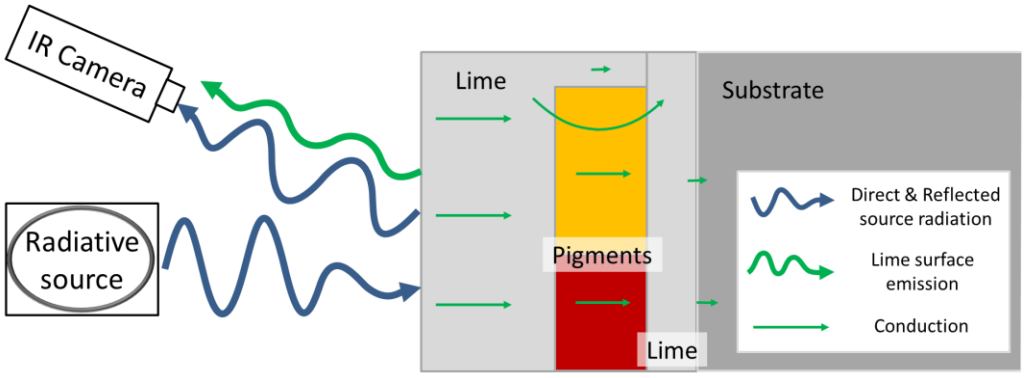

Figure 1: Sketch of the radiative-conductive flux conversion after heat stimulation of the surface by the blackbody radiation

2.2 Thermo-physical properties of mural paintings

In order to simulate the heat transfer inside a wall containing a hidden painting, the materials thermo-physical properties (thermal conductivity K, density ρ, Specific heat capacity C_p) of the materials must be determined. Several types of mural painting techniques have been used in history. The techniques of frescoes are always based on the overlapping of several layers: a substrate (wall), a plaster-like layer referred as *intonaco*, then pigments. There are different types of pigments and they may need a binder depending on the painting technique. The pigments are either applied on fresh *intonaco* (*buon fresco* technique) or on dry *intonaco* (*secco* technique). Contrary to *buon fresco*, the *secco* technique requires to mix the pigments with a binder. Ochres pigments are natural and were used since ancient times, and linseed were also widely used as a pigment binder. That is why those materials were chosen in this study.

The pigment-oil mixture is not referenced in literature, but it is possible to assess these properties from its composition. While the heat capacity and density can easily be assessed, the thermal conductivity of a liquid-rock medium is more complex to determinate. Robertson [27] gives a formula of the effective conductivity K_{eff}:

$$K_{eff} = K_f + \gamma^2 \left[\left(K_r + p(K_{min} - K_r)\right) - K_f\right] \quad (1)$$

where K_f, $K_r$and $K_{min}$are respectively the fluid, the rock (for zero percent quartz or other minerals) and the mineral conductivities in W/mK, p is the fraction of the mineral among the rock solid phase. The term γ called solidity is the fraction of the solid volume over the total volume. It is related to porosity ϕ, $\gamma = 1 - \phi$.

Ochres can have various compositions, especially regarding the provenance[28]. They are mostly composed of grains of quartz and other components. The color is given by different

iron oxyhydroxides and oxides: the red color indicates the presence of hematite while the yellow color is given by goethite[29]. Red and yellow ochres used in this study have been observed by microscope. The resulting photographs shown in Figure 2 reveal the crystals composition: white for quartz, yellow for goethite and red for hematite. As an approximation, the equivalent conductivity and other properties are calculated for a solid mixture of 80%quartz - 20%hematite ($p = 0.8$). The solidity γ of the ochre-oil painting can be evaluated with the close packing configuration $\gamma = 74\%$, as the excess of oil can be absorbed by the dry limewash. The properties of the primary materials are given from previous studies (hematite [30][27], quartz [27] [31], linseed oil [32][33]).

For the limewash, formula (1) is not relevant as the water is mostly evaporated after its application. Indeed, the limewash is prepared by mixing lime powder and water, with a high percentage of water. An increase of the water content in mixtures causes an increase of porosity as empty spaces are created in the structure due to the evaporation of the water excess[34]. It can be noticed that the dry lime-water mixture conductivity (0.27 W/mK) is lower than both the conductivities of water (0.6 W/mK) and limestone (2.1 – 3 W/mK) because of this evaporation. For our application to plaster walls, it must be noted that the properties of plaster and limewash are similar [20][22]. The other thermal properties were provided in references [34][35][36]. The lime mortar properties are given by [35] and [27]. The thermal properties of the selected materials for simulation are listed in Table 1. The diffusivity of quartz and hematite are relatively close, but the thermal properties of goethite are unknown. Ochres might also be composed of less conductive materials as kaolinite[37]. Despite these uncertainties, we can observe the trend that the painting diffusivity is strongly higher than that of limewash or substrate.

Materials		ρ kg/m^3	Cp J/(kgK)	K W/(mK)	α 10^{-7} m^2/s
Primary materials	Hematite (red)	5260	650	12,4	36,27
	quartz	2650	750	8,1	40,70
	vegetable oil	900	1800	0,17	1,05
Equivalent materials	Limewash (62% lime, 38%water)	905	890	0,27	3,35
	Lime mortar (41%lime, 41%sand, 18%water)	1914	800	0,12	0,78
	Ochre painting (74%rocks [80%quartz, 20%hematite], 26%oil)	2581	1008	6,7	25,62

Table 1: Thermal properties of materials used for the Finite Elements simulation

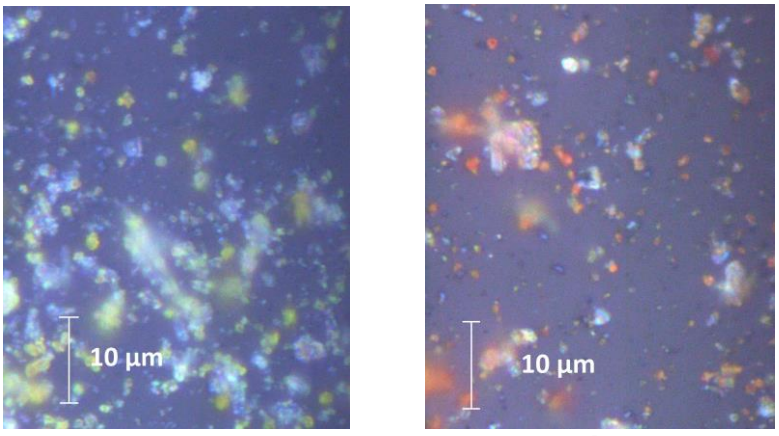

(a) (b)

Figure 2: Photomicrographs of the crushed ochre powder (a: yellow; b: red)

3. THERMAL MODELING

3.1 Thermal simulation conditions

In order to determine the surface temperature evolution needed to estimate the effect of heat stimulation on a hidden painting, a preliminary analysis is done using the FEM commercial software COMSOL Multiphysics. The geometry of a cross section of the considered sample is shown in Figure 3. The corresponding 2D model takes into account a thick lime mortar substrate layer; a thin limewash layer (0.2mm thick); an ochre painting (0.5mm thick) and finally, a limewash layer that covered all other layers. The thickness of the limewash on the painting is 0.5mm. The painting pattern represents 5 bands of variable width (from 2 to 12 mm) and different spacing in order to highlight the thermal spatial resolution of the method. A uniform heat flux of 650 W/m² is applied to the limewash surface corresponding to the heat flux radiated by the blackbody of 15 cm diameter at 500 °C placed at a distance of 35 cm from the sample and considering a sample emissivity of 0.9. The stimulation-heating flux is applied during 60 seconds. Figure 3 represents the painting pattern and the characteristic temperature field of the five embedded painting bands during thermal stimulation. It can be seen that the non-uniform material structure generates a non-uniform surface temperature during excitation.

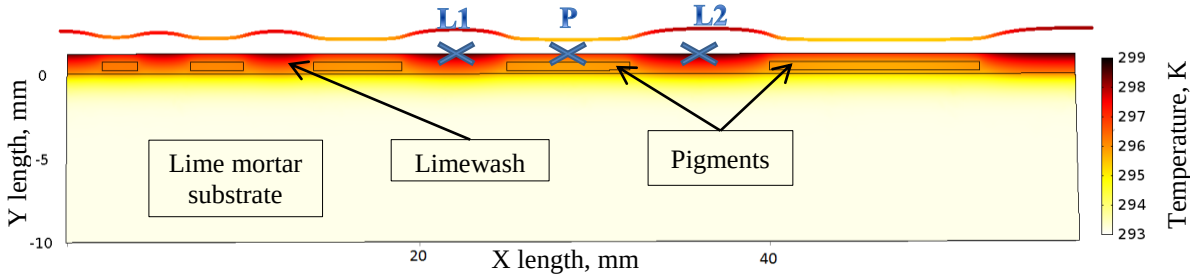

Figure 3: Simulated geometry domain and temperature field of the academic sample during thermal excitation and a temperature profile at the limewash surface (top); Location of 3 reference points, two at the surface over limewash (L1, L2) and one at the surface over hidden painting (P)

3.2 Definition of the sensibility and spatial resolution criteria

In order to characterize both the threshold detection capability and spatial resolution rendering of the method, the surface temperature response after the heat flux step has been computed. Figure 4 shows a plot of the temperature for the three surface reference points L1, L2 and P previously defined in Figure 3. The temperatures responses over lime at the two different locations besides the hidden painting (L1 and L2) are relatively close. At the very beginning of the heat flux stimulation, the temperature rise is the same for every point along the X axis as the thermal wave has not reached the heterogeneous zone (painting) yet. After this little time, namely around 0.4 seconds, as the painting is more conductive, it drains a higher flux towards the substrate, deeper in the sample thickness. As the heat flux is assumed equally distributed, the temperature at the surface over the painting is lower. A sketch of the temperature field and a profile at the sample surface during the heat rise is shown in Figure 3.

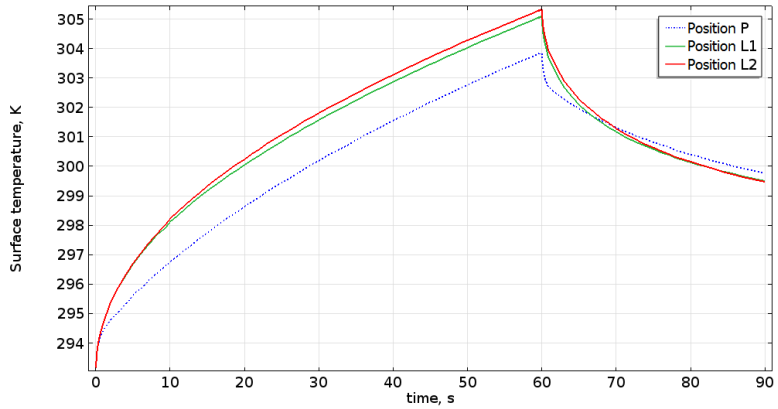

Figure 4: Surface stimulation temperature responses at three points: over only limewash (L1, L2) and over hidden painting (P)

After the end of the heat stimulation, the temperature quickly decreases and the surface temperature tends to be homogeneous. However, as the volumetric heat capacity ρC_p of the painting is higher than the limewash, its temperature decrease is slower and after a few seconds, the temperature at point P becomes higher than that of the points L1 and L2. This simple observation leads to the possibility of highlighting the presence of hidden paintings, using the transient effects.

In order to find the most relevant time to process the data, the simulated temperature differences have been analyzed. The absolute thermal contrast of the temperature has been defined at any time t as the difference between the variable $T(t)$ and the teperature at the reference time:

$$C(t) = T(t_{ref}) - T(t) \tag{2}$$

For simulation, the reference time t_{ref} was taken at $t = 60s$, the time value corresponding to the end of the heat stimulation. The surface temperature contrast $C(t)$ is plotted in Figure 5 at different times starting from the heat stimulation is finished. It can be noted that the temperature contrast can also be defined as a ratio, divided by the temperature difference at a reference position. This relative definition permits a direct comparison along time, but the present definition permits the contrast to be directly compared to the camera NETD.

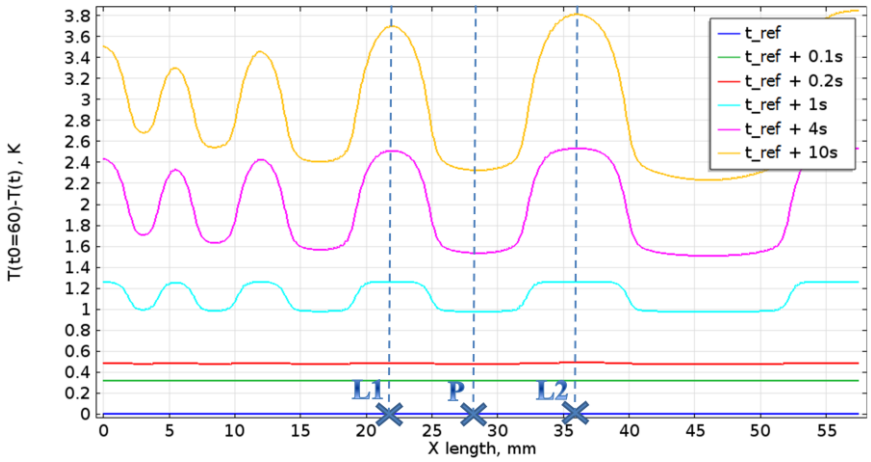

Figure 5: Simulated absolute thermal contrast function along the surface over the buried painting patterns for different times after the end of the thermal stimulation

The temperature contrast at the surface clearly reveals the presence of the embedded painting. A quantitative criterion to evaluate the thermal sensibility of the method has been expressed

as the difference of the temperature contrast between both points at the surface: over the pigments P and over limewash L1.

$$\Delta C = \left(T_{s_P}(t_{ref}) - T_{s_P}(t)\right) - \left(T_{s_{L1}}(t_{ref}) - T_{s_{L1}}(t)\right) \quad (3)$$

ΔC is expressed in Kelvin and corresponds to the absolute difference of signal between two characteristic surface points (located above hidden pigments or not) in terms of temperature contrast. It can be calculated at any time, and is plotted in Figure 6a, after the end of the thermal stimulation. Using this criterion, the relative thermal sensibility $\Delta C/C$ has also been defined by making the ratio between the thermal sensibility ΔC and the reference contrast, at the point P over painting:

$$\frac{\Delta C}{C} = \frac{\left(T_{s_P}(t_{ref}) - T_{s_P}(t)\right) - \left(T_{s_{L1}}(t_{ref}) - T_{s_{L1}}(t)\right)}{\left(T_{s_P}(t_{ref}) - T_{s_P}(t)\right)} \quad (4)$$

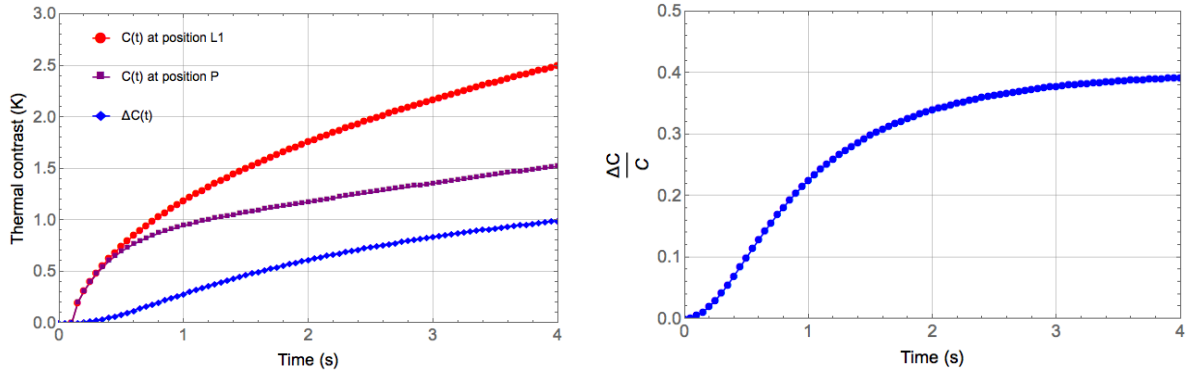

(a) (b)

Figure 6: Temperature contrast $C(t)$ for two points at the surface (over a 7mm wide band and over simple limewash) and the corresponding thermal sensibility of the method in blue (a: absolute ΔC; b: relative $\Delta C/C$)

The absolute and the relative thermal sensibility ΔC and $\Delta C/C$ are reported for some time values in Table 2. These results express the ability of the method to detect embedded painting layers into a wall. Indeed, the MWIR thermal imager used in this study was designed for high performing thermal imaging. It has a Noise Equivalent Temperature Difference (NETD) of about 20 mK. When the thermal sensibility ΔC exceeds this value quite quickly, for instance when t_{ref}+0.27s (see results in Table 2), then the method detection threshold can be considered achieved. Furthermore, it can be observed that even if the reference time is not set immediately at the end of the heat stimulation, there is a time delay of a few hundreds of milliseconds before the thermal sensibility substantially increases. The maximum sensibility ΔC corresponding to this 7 mm wide painting band reaches a value of 1.5 K after 20 seconds. This thermal sensibility is more important for larger painting bands, but even for narrow bands, the contrast remains significantly measurable (ΔC= 0.6 K for the 2 mm wide band). It can be noted that after a few seconds, the thermal sensibility ΔC stagnates while the temperature contrast at both positions still increases. That is why a maximum value of the relative sensibility $\Delta C/C$ is observed, at around t_{ref}+5s (39.3%).

t, s	t_{ref}	t_{ref}+0.1s	t_{ref}+0.2s	t_{ref}+0.5s	t_{ref}+1s	t_{ref}+4s	t_{ref}+10s	t_{ref}+20s
ΔC(t) , K	0	0.002	0.010	0.085	0.284	0.976	1.376	1.491
ΔC/C (t)	x	0.6 %	2.0 %	10.0 %	22.6 %	38.9 %	37.2 %	31.5 %

Table 2: Simulated results of the absolute and relative thermal sensibility of the method for different times after the heat stimulation end

The thermal sensibility is not the only parameter that should be considered to establish the spatial resolution characterization of the method. Another important observation is the shape of the contrast profiles at the surface over time. Indeed, those profiles, though with more and more important amplitude, are also more and more distorted by heat diffusion inside the solid. In order to take the degradation of the painting delimitation into account, we have stated a second criterion. This new spatial thermal resolution criterion is defined as the effective width of the detected subsurface band, considering the spatial derivative of the contrast. The relative criterion $\Delta L/L$ has been expressed as:

$$\frac{\Delta L}{L} = \frac{x_b - x_a}{l_{band}} \tag{5}$$

With a and b such as

$$\begin{cases} \left(\frac{\partial T}{\partial x}\right)_a / \max\left(\frac{\partial T}{\partial x}\right) = -0.1 \\ \left(\frac{\partial T}{\partial x}\right)_b / \max\left(\frac{\partial T}{\partial x}\right) = +0.1 \end{cases} \tag{6}$$

Using this definition, the relative thermal resolution criterion $\Delta L/L$ has been computed and plotted in Figure 7. It is established that this criterion value decreases inversely with the time difference $\Delta t = t - t_{ref}$ after the end of the heat stimulation. Δt is also referred as processing time. The paintings contours appear more smoothed as Δt increases. Furthermore, it is observed that the bands without painting are especially affected by the distortion of the contrast profiles due to thermal diffusion. The profiles keep degenerating over time and the thinner the band, the harder it is affected. The painting pattern will never be as clear as it is shortly after t_{ref}.

Without any consideration of this spatial criterion, one would think to compute the thermal contrast as long after the stimulation as possible. However, this criterion does not take into account the amplitude of the thermal contrast which must be sufficiently high to be detected by the thermal imager. Thus, in all cases, the absolute sensibility ΔC must be compared to the camera detectability to determine the possibility of the painting detection. Considering the two criteria $\Delta C/C$ and $\Delta L/L$, there is an optimum time (in our configuration, around $t_{ref} + 0.5\ s$) for the choice of the time to process the surface temperature contrast $C(t)$. Right after the end of the thermal stimulation, the thermal sensibility is too low; too long after the stimulus end, the thermal contrast pattern is too distorted.

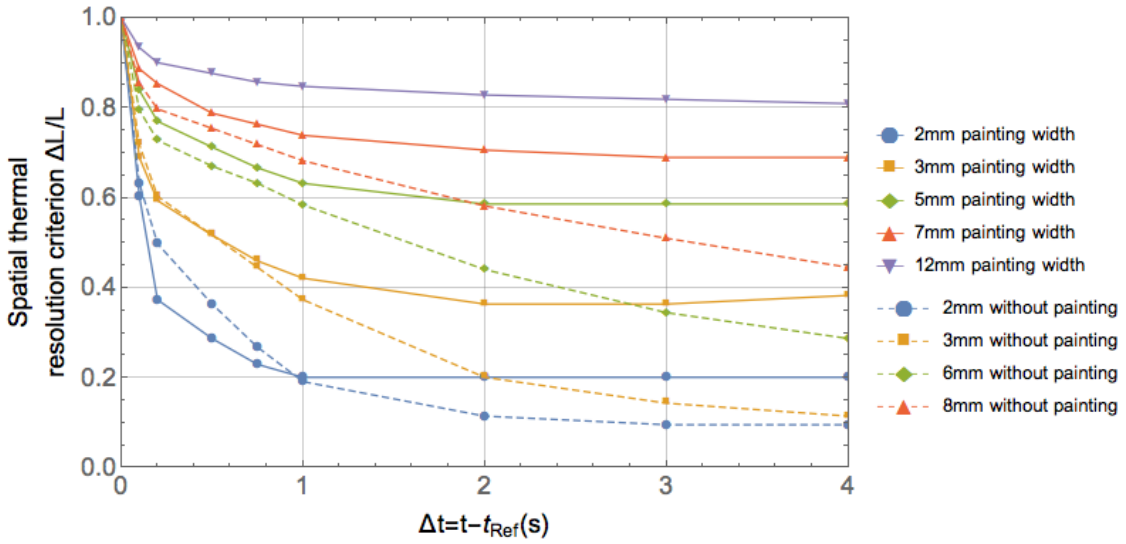

Figure 7: Spatial thermal resolution criterion $\Delta L/L$ for different widths of bands with or without painting, function of the processing time Δt

3.3 Sensitivity study of the painting thermo-physical properties and depth

As explained in section 2.2, the thermal properties can vary a lot considering the materials composition of the wall (mortars preparation, nature and provenance of pigments). A sensitivity study was carried out to evaluate the influence of both the effective thermal conductivity and specific heat capacity values of the painting on the thermal contrast. Indeed, the thermo-physical properties K and C_p could be strongly varied around our estimation values, respectively 6.7 W/mK and 1008 J/kgK. The thermal sensibility ΔC is shown in Figure 8 for different values of these two parameters at the time $t = t_{ref} + 1$. For no variation (Parameter/Parameter$_0$ = 1), the value 0.284 K is found. It appears that the detection method is more sensible to the painting heat capacity. As the thermal sensibility remains high compared to measurement threshold (ΔC>50 mK even for a $\pm$90% variation of the heat capacity value), the painting should still be detectable for a significantly different painting composition.

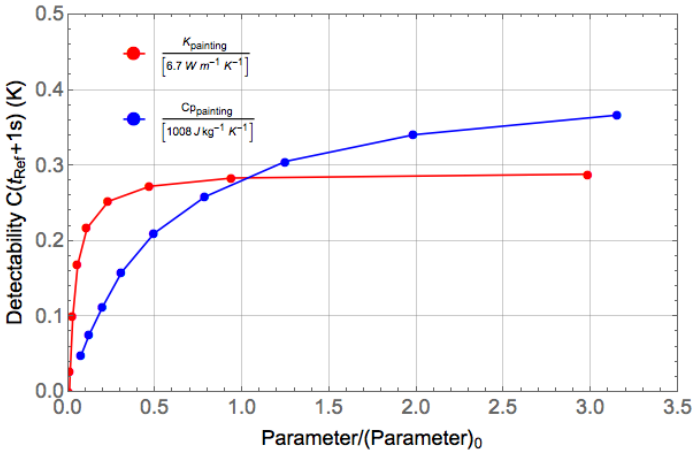

Figure 8: Sensitivity analysis of the sensibility ΔC at $t = t_{ref} + 1s$ for the painting thermal properties: conductivity K and specific heat capacity C_p

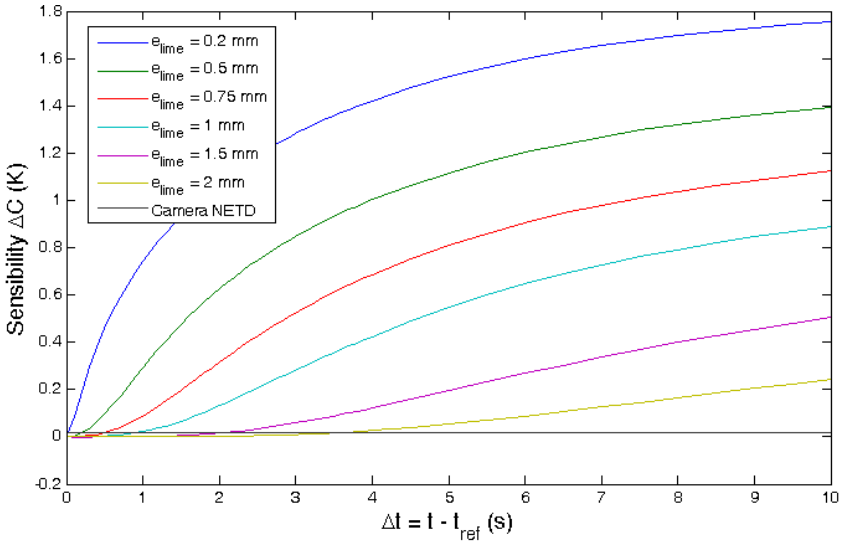

Figure 9: Thermal sensibility as a function of time for several limewash thicknesses

The sensitivity of the method to the lime thickness, e.g. the painting depth, was also investigated. The variation of the sensibility ΔC in time must be considered since the optimum processing time is clearly dependent on the processing time Δt. Indeed, the characteristic heat conduction time increases with the square of the lime thickness e_{lime}. Also, the deeper the painting is, the more distorted the contrast profile will be. For a 2 mm

thickness, the painting should be detected as the sensibility reaches $\Delta C = 0.24\ K$ for $\Delta t = 10\ s$; for a 4 mm thickness, the sensibility is 80 mK for $\Delta t = 30s$.

4. EXPERIMENTAL SETUP AND RESULTS

4.1 Sample preparation

A sample reproducing a target pattern fresco was realized to validate experimentally our simulations analysis. A photograph of the painting before and after the covering process is provided in Figure 11(a) and (b). A lime mortar (lime and sand with a 1:2 proportion diluted in water) was preliminary produced to form the substrate of the sample, comparable to an *arriccio* of 2 cm thickness. A very thin limewash layer (lime and water) was then applied as a simple *intonaco*. The pigments were painted on this limewash layer after being dried; this corresponds to the *secco* technique. Red ochre and yellow ochre (from France) mixed with linseed oil were used as painting. The painting bands (3 to 15 mm wide) were drawn through a specifically designed stencil and were dried for several days before being covered by three thin limewash layers. The limewash was at last sanded to obtain a plane surface. The covering layer is about 0.5 mm thick and the painting layer is a few hundreds of microns thick. The layout of the test painting represents bars and has been designed to assess for our method:

- the ability to detect the presence or the absence of an underneath pigment (left side of the pattern in Figure 11a)
- the ability to distinguish two pigments of different nature (right side of the pattern in Figure 11a)
- the length resolution limit of a painted line detection

4.2 Experimental setup and procedure

The radiation emitted by a blackbody of 15 cm diameter aperture with a 0.99 emissivity, finely regulated at 500 °C, was used to thermally stimulate the sample. A large mechanical shutter was employed to monitor both the thermal excitation start and end. To record thermograms of the sample surface, a commercial MWIR camera with high resolution was used. It was an InSb FPA thermal imager well suited for the 1.5 to 5 µm wavelength band. The camera thermal sensibility is about 4 mK per digital level (MRTD) and its NETD is 20 mK. This camera permits to work at high frequency. The acquisition frequency was 100 Hz for a full frame rate. A picture of the experimental setup can be seen in Figure 10.

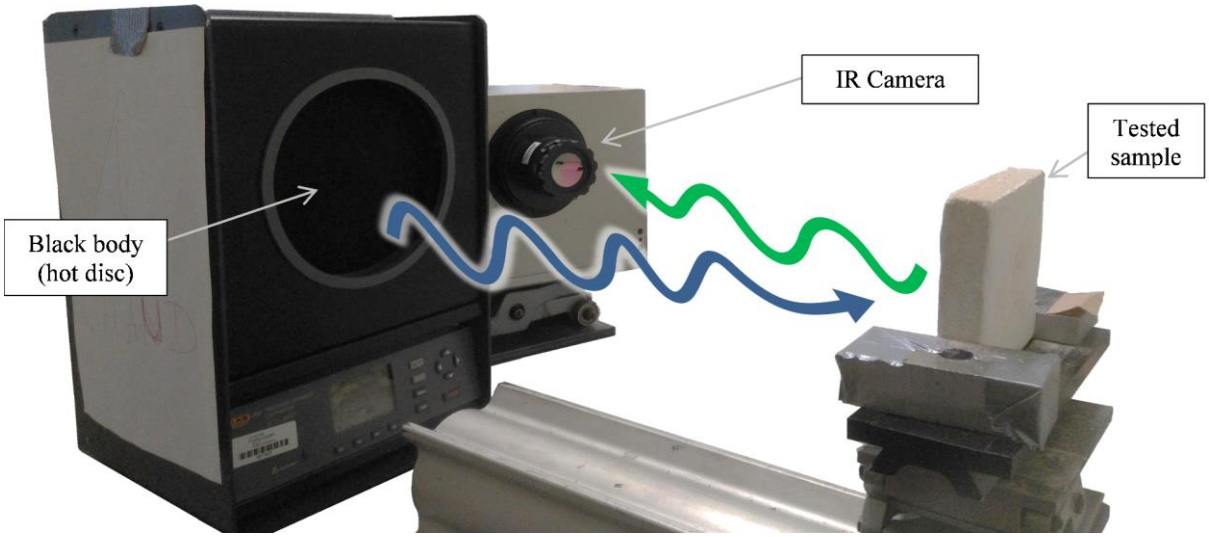

Figure 10: Experimental set-up: black body, painting sample, and the infrared camera

(a) (b) (c)

Figure 11: Photographs of the painting sample before (a) and after (b) covering it with the limewash layer; greyscale image of the experimental thermal contrast $C^{i,j}_{t=t_{ref}+0.5s}$ using the cooling-down thermal imaging method (c)

In order to avoid the reflection of the infrared heat flux stimulation, the acquisition must then be done when the source is obstructed. The image processing was realized from the frame sequence at the moment when the heat stimulation was stopped, as indicated in Figure 12a. Figure 12b shows the transient cooling-down thermal emission acquired by the camera. To avoid missing the cooling down start, the acquisition was pre-triggered. The frames corresponding to this pre-triggered period are saturated due to the mid-infrared blackbody radiation reflected on the surface sample. The exposure time was then chosen relatively long to increase the digital levels (DL) pixel values but also short enough to enable a high sample rate and to be able to set an accurate time reference t_{ref}. The sharp decrease corresponds to the blackbody obstruction, which takes around 0.3 s to be shut. As shown in Figure 6, this delay should not affect badly the thermal sensibility ΔC, but it explains why the thermal image of the pattern can be obtained experimentally more quickly than predicted by the simulations. As a consequence of this shuttering, the reference time is set after the end of the

effective stimulus end. This delay has an influence for the very beginning of the cooling down. The slow decrease, which occurs after the end of the shuttering (from 1.77s for the recorded signal time), is due to the actual temperature decrease of the sample surface, as seen in simulation (Figure 4).

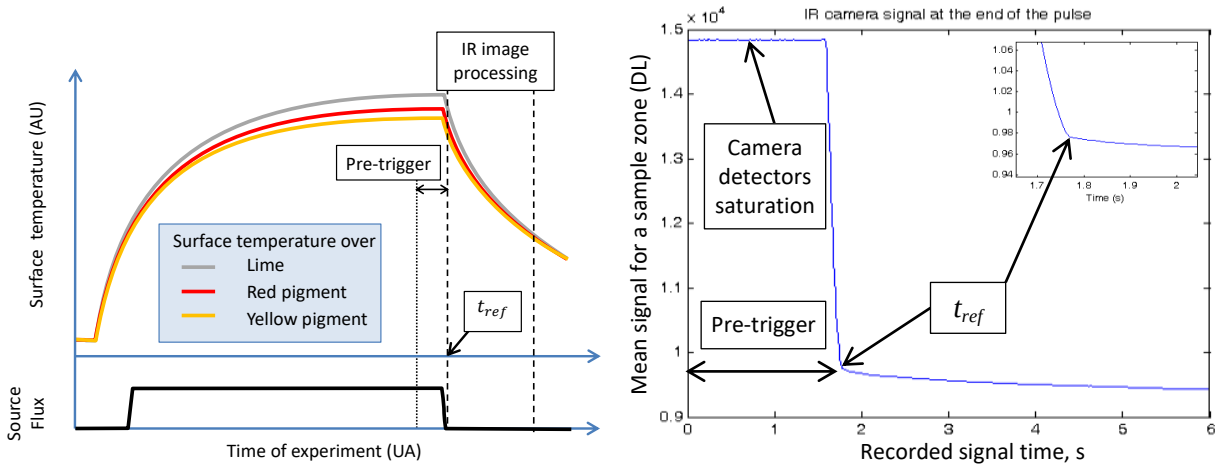

(a) (b)

Figure 12: Thermogram schema showing the experimental procedure (a); Mean signal response of the camera signal around the end of the thermal stimulation (b)

Data processing consists in computing the thermal contrast function from the camera signal of every pixel $S_t^{i,j}$. The thermal contrast function has been defined as the difference of the signal at any time t with a constant reference, as presented before in equation (2). The time reference is therefore chosen as close as possible as the source covering ($t_{ref} = t_{source\_covering}$) defining the end of the heat stimulation. Finally, the camera signal has been time-averaged in order to significantly reduce the temporal noise. The resulting averaged contrast $C_t^{i,j}$ affected to the pixel (i, j) at the time t is defined by the following equation:

$$C_t^{i,j} = \frac{1}{10}\sum_{t_0=t_{ref}}^{t_{ref}+\frac{9}{f}} S_{t_0}^{i,j} - \frac{1}{10}\sum_{t_0=t}^{t+\frac{9}{f}} S_{t_0}^{i,j} \quad (7)$$

4.3 Experimental results on the test painting sample

Proceeding as described above, we aim at experimentally validating both the recovery method and the two proposed detection criteria. Figure 13 shows two frames of the camera raw sequence data recorded at two different times of the excitation stimulus: at the stimulation end t_{ref} and after 0.5 seconds. The region of interest of the frame is a rectangle of 192x234 pixels. From those images it is possible to see some surface effects, but the painting pattern remains invisible. Even if the surface was sanded and seems planar, there are surface roughnesses which induce variations in directional emissivity and reflectivity. Without thermal imaging processing the buried painting layers do not appear.

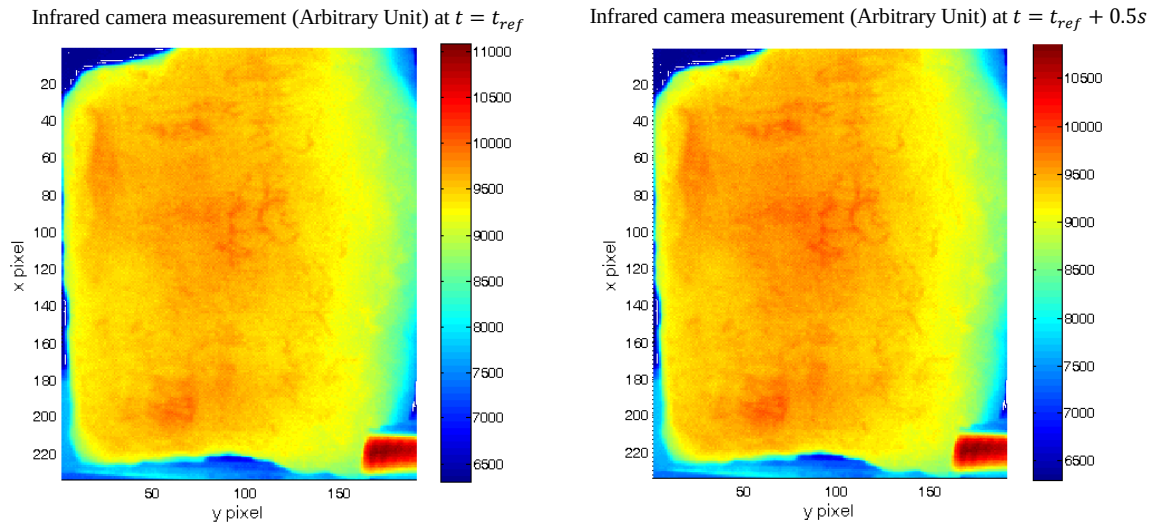

Figure 13: Infrared camera measurements in color scale at the end of the thermal stimulation (a) and after one second (b)

We have then processed the recorded infrared video sequence by computing the thermal contrast images using equation (7). To illustrate the results, Figure 11 displays several pictures representing the painting sample to be detected before it was recovered by the limewash (a), after the painted pattern was hidden (b) and finally the processed thermal contrast image computed as previously described (c). This thermal image corresponds to the processed contrast field $C^{i,j}_{t=t_{ref}+0.5s}$ 0.5 seconds after the stimulation end, in a gray scale. The resulting thermal image shows a good reconstitution of the painting pattern. First, the presence or absence of pigments is clearly revealed, according to the left part of the pattern. What is more noteworthy is the fact that we can distinguish two shades in the right side. It is thus possible to make the difference between two pigments, between the two kinds of ochre at least. Finally, almost all the pattern edges are visible. Only the two last painting bands at the bottom are not well marked. The detection length threshold is thus relatively low for our configuration as it is possible to detect a 4 mm painting band.

In order to illustrate the influence of the processing time Δt value, Figure 14 shows the contrast at different times of the cooling down. For the studied sample, the best contrast time is difficult to determine. The general pattern is well reconstructed a few seconds after the end of the stimulation. However, for shorter times ($t_{ref} + 0.1s$ to $t_{ref} + 1s$), the signal pattern edges are sharper and the lines are thinner. This is in good agreement with the simulated contrast profiles plotted in Figure 5 and the spatial resolution criterion plotted in Figure 7. It can be noted that some patterns appear from $t_{ref} + 0.1s$. As the stimulus is not immediately ended and the experimental reference time is set at the end of the shuttering time, it implies a delay in the reference time. The experimental thermal sensibility then reaches more quickly the camera detectability. The painting patterns might also appear less clear for longer Δt than a few seconds because of the noise of the ambient radiations. These radiative perturbations justify the choice of a short Δt, as soon as the signal emerges from the camera noise. The camera noise represents about 4 digital levels, and it can be seen on Figure 14 (a and b) that this emergence is not clear for the shortest Δt.

In order to finally evaluate the spatial resolution of the method we have plotted in Figure 15 several contrast profiles along a line perpendicular to the painting bands. These presented profiles are averaged on 20 pixel adjacent lines; the corresponding data zone is shown as the

red rectangle in Figure 14d. These profiles are given at characteristic times so they can be compared to the temperature contrast profiles in Figure 5. In the same plot appear as the dotted line the painting edges, corresponding to the stencil design.

The correspondence with the painting presence is visible even for the thinner band of 3 mm. Like the simulated temperature contrast, the signal contrast above both painting bands is found smaller than on the zones where there is only limewash. Also, the experimental contrast profiles for short times ($t_{ref} + 0.1s$ to $t_{ref} + 1s$) highlight more clearly the painting limits while the longer times profiles are more smoothed but of higher amplitudes. The simulated temperature and experimental signal profiles are thus in good agreement.

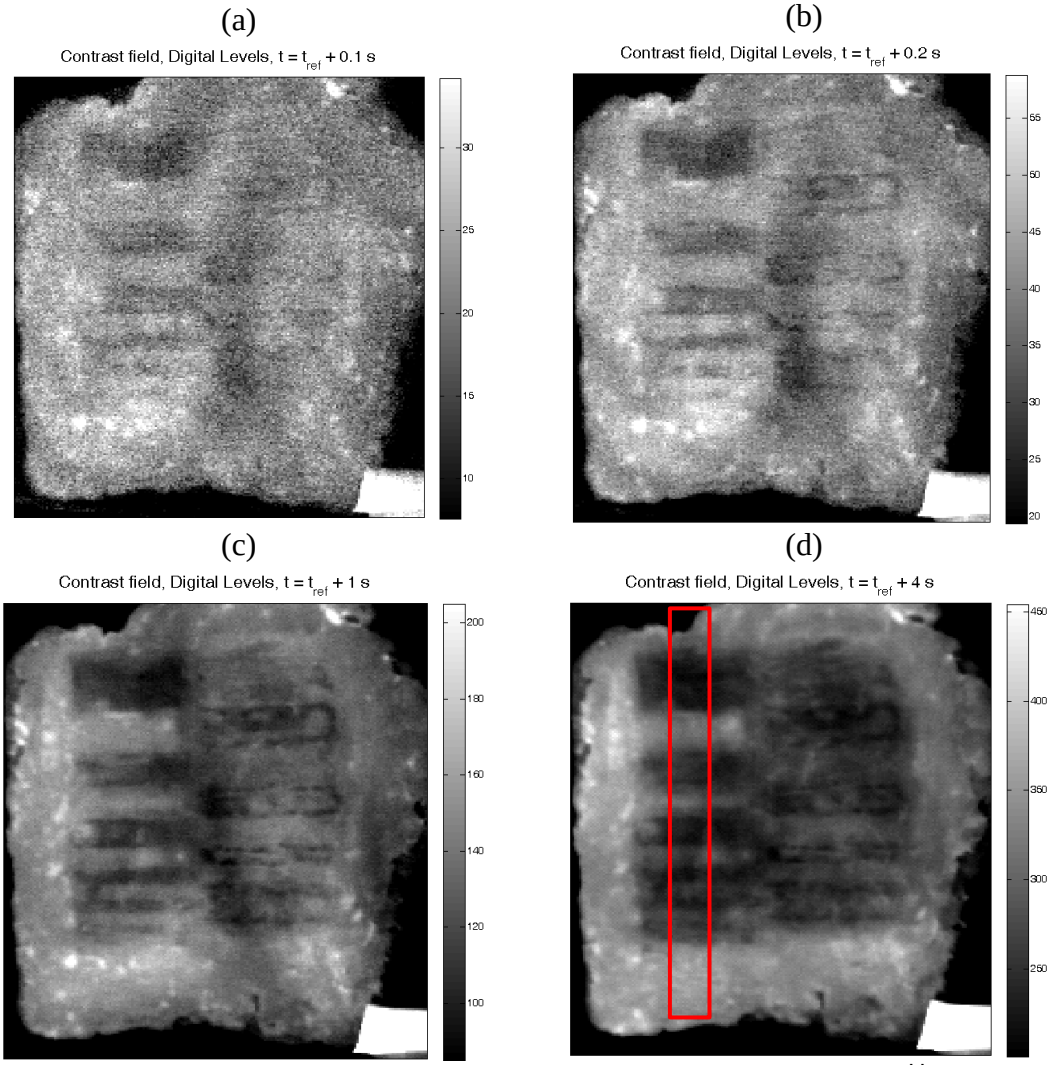

Figure 14: Paintings pattern experimentally revealed using the contrast function $C_t^{i,j}$ at different processing time Δt (0.1s, 0.2s, 1s, 4s) of the infrared sequence

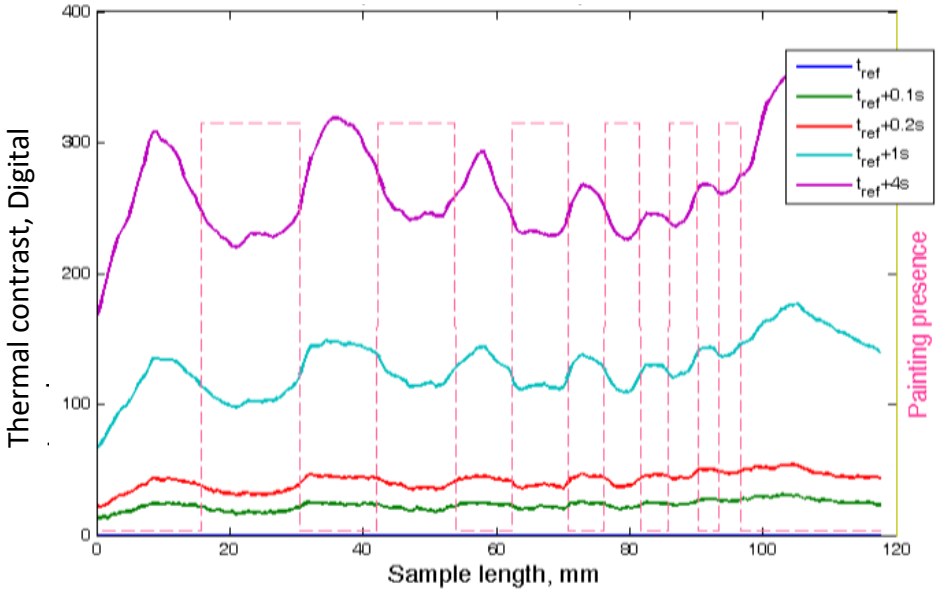

Figure 15: Experimental contrast profiles along the surface for different times after the end of the thermal stimulation showing the increase of the thermal contrast amplitude and the deterioration of the spatial resolution over the processing time Δt

5. CONCLUSIONS AND PROSPECTS

In this paper, a cooling-down technique to detect the presence of a fresco covered by a limewash or plaster layer was developed. This non-destructive technique is based on the analysis of the transient heat diffusion inside a plastered wall just after the end of infrared radiation stimulation. Both the thermal sensibility of the method and the spatial resolution of the revealed pattern are analyzed along the time of the processed sequence.

Simulations have shown that the thermal imager resolution of 20 mK is significantly lower than the thermal contrast difference, up to 1.5 K for a 7 mm wide painting band placed at a 0.5 mm depth. Simulations have also permitted to study the spatial distortion of the pattern resulting from the heat diffusion. A new spatial resolution criterion has been stated to set the best processing time to obtain the sharpest thermal contrast image. Thus, the results have shown that both the thermal sensibility and the spatial resolution of the method must be taken into account to find the optimal time value to compute the thermal contrast image from the infrared sequence. Using the two criteria, a very sharp thermal image giving the best definition of the pattern could be obtained.

For experimentation purposes, a covered painting sample was realized. Reconstituted images of mural samples covered by a limewash layer were shown. Not only the general painting pattern was revealed, but two ochre pigments of different nature were distinguished. The presence of narrow painting bands down to 3 mm width could be highlighted. The experimental and simulation analyses of the thermal contrast are in good agreement.

The proposed method is promising for two reasons. The first one is that a unique thermal stimulation was considered while periodic thermography would highly reduce the noise-to-signal ratio. The second is the typical absolute thermal contrast, considerably higher than the camera detectability. This method could then be improved to probe walls where frescoes have been covered by a limewash or plaster layer of a typical thickness up to a few millimeters.

Since limewash and plaster, having similar thermal properties, are often used to hide murals, this application represents a major interest for both curators of historical monuments and

other actors of heritage. Also, the present study might be useful for various detection problems such as the inspection of defaults in materials for which the defined criteria might be applied.

6. REFERENCES

[1] H. Liang, R. Lange, H. Howard, and J. Spooner, "Non-invasive investigations of a wall painting using optical coherence tomography and hyperspectral imaging," 2011, vol. 8084, p. 80840F–80840F–7.

[2] E. Cheilakou, M. Troullinos, and M. Koui, "Identification of pigments on Byzantine wall paintings from Crete (14th century AD) using non-invasive Fiber Optics Diffuse Reflectance Spectroscopy (FORS)," *J. Archaeol. Sci.*, vol. 41, pp. 541–555, Jan. 2014.

[3] C. Clementi, V. Ciocan, M. Vagnini, B. Doherty, M. L. Tabasso, C. Conti, B. G. Brunetti, and C. Miliani, "Non-invasive and micro-destructive investigation of the Domus Aurea wall painting decorations," *Anal. Bioanal. Chem.*, vol. 401, no. 6, pp. 1815–1826, Jul. 2011.

[4] C. Daffara, S. Parisotto, and P. I. Mariotti, "Mid-infrared thermal imaging for an effective mapping of surface materials and sub-surface detachments in mural paintings: integration of thermography and thermal quasi-reflectography," in *SPIE Optical Metrology*, 2015, p. 95270I–95270I.

[5] D. Giovannacci, V. Detalle, D. Martos-Levif, J. Ogien, E. Bernikola, V. Tornari, K. Hatzigiannakis, K. Mouhoubi, J.-L. Bodnar, G.-C. Walker, D. Brissaud, B. Trichereau, B. Jackson, and J. Bowen, "Case study of Sainte-Marie Chapel, Fontaine Chaalis (France): complementarity of different optical techniques," in *SPIE Optical Metrology*, 2015, p. 95270L.

[6] E. Grinzato, C. Bressan, S. Marinetti, P. G. Bison, and C. Bonacina, "Monitoring of the Scrovegni Chapel by IR thermography: Giotto at infrared," *Infrared Phys. Technol.*, vol. 43, no. 3–5, pp. 165–169, Jun. 2002.

[7] J. L. Bodnar, J. C. Candoré, J. L. Nicolas, G. Szatanik, V. Detalle, and J. M. Vallet, "Stimulated infrared thermography applied to help restoring mural paintings," *NDT E Int.*, vol. 49, pp. 40–46, Jul. 2012.

[8] C. Daffara, D. Ambrosini, L. Pezzati, and D. Paoletti, "Thermal quasi-reflectography: a new imaging tool in art conservation," *Opt. Express*, vol. 20, no. 13, p. 14746, Jun. 2012.

[9] D. Ambrosini, C. Daffara, R. Di Biase, D. Paoletti, L. Pezzati, R. Bellucci, and F. Bettini, "Integrated reflectography and thermography for wooden paintings diagnostics," *J. Cult. Herit.*, vol. 11, no. 2, pp. 196–204, Apr. 2010.

[10] D. Gavrilov, C. Ibarra-Castanedo, E. Maeva, O. Grube, X. Maldague, and R. Maev, "Infrared methods in noninvasive inspection of artwork," in *Proceedings of 9th international conference on NDT of art*, 2008, pp. 25–30.

[11] G. C. Walker, J. B. Jackson, D. Giovannacci, J. W. Bowen, B. Delandes, J. Labaune, G. Mourou, M. Menu, and V. Detalle, "Terahertz analysis of stratified wall plaster at buildings of cultural importance across Europe," 2013, vol. 8790, p. 87900H–87900H–8.

[12] J. B. Jackson, M. Mourou, J. F. Whitaker, I. N. Duling, S. L. Williamson, M. Menu, and G. A. Mourou, "Terahertz imaging for non-destructive evaluation of mural paintings," *Opt. Commun.*, vol. 281, no. 4, pp. 527–532, 2008.

[13] G. P. Gallerano, A. Doria, E. Giovenale, G. Messina, A. Petralia, I. Spassovsky, K. Fukunaga, and I. Hosako, "THz-ARTE: non-invasive terahertz diagnostics for art

conservation," in *33rd International Conference on Infrared, Millimeter and Terahertz Waves, 2008. IRMMW-THz 2008*, 2008, pp. 1–2.
[14] X. Maldague and P. Moore, "Nondestructive testing handbook–infrared and thermal testing American Society for Nondestructive Testing," *OH USA*, 2001.
[15] R. Montanini and F. Freni, "Non-destructive evaluation of thick glass fiber-reinforced composites by means of optically excited lock-in thermography," *Compos. Part Appl. Sci. Manuf.*, vol. 43, no. 11, pp. 2075–2082, 2012.
[16] J. R. J. van Asperen de Boer, "Infrared Reflectography: a Method for the Examination of Paintings," *Appl. Opt.*, vol. 7, no. 9, p. 1711, Sep. 1968.
[17] C. Ibarra-Castanedo, M. Genest, J.-M. Piau, S. Guibert, A. Bendada, and X. P. Maldague, "Active infrared thermography techniques for the nondestructive testing of materials," *Capter XIV Book"Ultrasonic Adv. Methods Nondestruct. Test. Mater. Charact. Ed Chen CH*, pp. 325–348, 2007.
[18] S. Marinetti, Y. A. Plotnikov, W. P. Winfree, and A. Braggiotti, "Pulse phase thermography for defect detection and visualization," in *Nondestructive Evaluation Techniques for Aging Infrastructures & Manufacturing*, 1999, pp. 230–238.
[19] W. B. Larbi, C. Ibarra-Castanedo, M. Klein, A. Bendada, and X. Maldague, "Experimental comparison of lock-in and pulsed thermography for the nondestructive evaluation of aerospace materials," in *6 th International Workshop, Advances in Signal Processing for Non Destructive Evaluation of Materials (IWASPNDE), Ontario, Canada. Citeseer*, 2009.
[20] N. P. Avdelidis and A. Moropoulou, "Applications of infrared thermography for the investigation of historic structures," *J. Cult. Herit.*, vol. 5, no. 1, pp. 119–127, Jan. 2004.
[21] P. Theodorakeas, C. Ibarra-Castanedo, S. Sfarra, N. P. Avdelidis, M. Koui, X. Maldague, D. Paoletti, and D. Ambrosini, "NDT inspection of plastered mosaics by means of transient thermography and holographic interferometry," *NDT E Int.*, vol. 47, pp. 150–156, Apr. 2012.
[22] P. Theodorakeas, N. P. Avdelidis, E. Cheilakou, and M. Koui, "Quantitative analysis of plastered mosaics by means of active infrared thermography," *Constr. Build. Mater.*, vol. 73, pp. 417–425, Dec. 2014.
[23] F. Lopez, V. de Paulo Nicolau, C. Ibarra-Castanedo, and X. Maldague, "Thermal–numerical model and computational simulation of pulsed thermography inspection of carbon fiber-reinforced composites," *Int. J. Therm. Sci.*, vol. 86, pp. 325–340, Dec. 2014.
[24] C. Ciocia and S. Marinetti, "In-situ emissivity measurement of construction materials," in *Proceedings of 11th Quantitative Infrared Thermography conference, paper QIRT2012-168, Naples (Italy)*, 2012.
[25] T. Davin, X. Wang, A. Chabane, R. Pawelko, G. Guida, B. Serio, and P. Hervé, "Thermal imaging method to visualize a hidden painting thermally excited by far infrared radiations," 2015, p. 95270T.
[26] P. Hervé, N. Rambure, S. Mattei, J. Oliveires, and J.-L. Bodnar, "Caractérisation spectrale par émission et transmission de revêtements dans l'infrarouge lointain: Application à l'analyse des tableaux," in *Actes du colloque" mesures optiques pour l'industrie*, 2007, vol. 20.
[27] E. C. Robertson, "Thermal properties of rocks," U.S. Geological Survey, USGS Numbered Series 88-441, 1988.
[28] J. C. Hughes and A. Solomon, "A preliminary study of ochres and pigmentaceous materials from KwaZulu-Natal, South Africa: towards an understanding of San pigment and paint use," *South. Afr. Humanit.*, vol. 12, no. 0, pp. 15–31, 2000.

[29] D. Hradil, T. Grygar, J. Hradilová, and P. Bezdička, “Clay and iron oxide pigments in the history of painting,” *Appl. Clay Sci.*, vol. 22, no. 5, pp. 223–236, Apr. 2003.
[30] T. J. Ahrens, *Rock physics & phase relations: a handbook of physical constants*. American Geophysical Union, 1995.
[31] K. Horai, “Thermal conductivity of rock-forming minerals,” *J. Geophys. Res.*, vol. 76, no. 5, pp. 1278–1308, 1971.
[32] A. K. Agarwal and L. M. Das, “Biodiesel development and characterization for use as a fuel in compression ignition engines,” *J. Eng. Gas Turbines Power*, vol. 123, no. 2, pp. 440–447, 2001.
[33] Y. Bertrand, L. . Hoang, and G. Valentin, “Vegetable oils as a substitute for mineral insulating oils,” MatPost, 2nd European Conference on HV & MV Substation Equipment, 2003.
[34] M. Stefanidou, M. Assael, K. Antoniadis, and G. Matziaroglou, “Thermal Conductivity of Building Materials Employed in the Preservation of Traditional Structures,” *Int. J. Thermophys.*, vol. 31, no. 4–5, pp. 844–851, May 2010.
[35] M. M. Barbero-Barrera, A. García-Santos, and F. J. Neila-González, “Thermal conductivity of lime mortars and calcined diatoms. Parameters influencing their performance and comparison with the traditional lime and mortars containing crushed marble used as renders,” *Energy Build.*, vol. 76, pp. 422–428, Jun. 2014.
[36] L. Eppelbaum, I. Kutasov, and A. Pilchin, “Thermal Properties of Rocks and Density of Fluids,” in *Applied Geothermics*, Springer Berlin Heidelberg, 2014, pp. 99–149.
[37] J.-M. Triat, *Les ocres*. CNRS éd., 2010.